Preparation of Homogeneous, Bulk Nanocrystalline Ni/Mo Alloys with Tripled Vickers Hardness Using Flame-Made Metal Nanoparticles

Evagelos K. Athanassiou, Robert N. Grass, Neil Osterwalder, and Wendelin J. Stark*

Institute for Chemical and Bioengineering, ETH Zurich, Wolfgang-Pauli str. 10, 8093 Zurich, Switzerland

Received April 24, 2007. Revised Manuscript Received July 20, 2007

Metals and metal−alloys have been traditionally prepared by large-scale reduction and ore refining. The present work demonstrates how this reduction and alloying step can be executed within flame aerosol reactors on a sub-second time scale and gives access to metal−alloy nanoparticles of 10−50 nm size at high production rate. We demonstrate the preparation of Ni/Mo and Hastelloy like metal nanoparticles as examples for this process and showed that the product particles exhibited an exceptionally high air stability and narrow particle size distribution in comparison to presently accessible materials. Sintering and compaction gave access to centimeter-sized bulk nanocrystalline alloys with strongly enhanced Vickers hardness. The versatility of already broadly used aerosol processing of oxides suggests that the extension of flame synthesis to metals and alloys may offer an alternative for the preparation of multicomponent nanocrystalline metals.

Introduction

Nanocrystalline metals and alloys have attracted considerable attention due to their exceptional electrical, magnetic, and mechanical properties.[1−5] During the past few years nanocrystalline materials have become available for a large range of applications. They have traditionally been produced by high-energy ball-milling[6] and cryomilling.[7] The energy consumption and the wear impurities introduced by the milling tools have motivated the design of other production methods such as electrodeposition,[8−10] thermal spray processes,[11] crystallization of amorphous metals,[12] inert gas condensation,[13,14] laser vaporization controlled condensation method,[15−17] wet phase,[18] and most recently reducing flame spray synthesis.[19,20] The continuous, gas-phase-based plasma, laser, or flame processes appear suitable[21] for large-scale production[22] since these processes have been derived from industrial flame aerosol processing as currently used for the manufacturing of several megatons of silica, titania, and carbon black nanoparticles.

Within the broad research interest on nanocrystalline materials, nickel−molybdenum-based alloys have been intensively investigated for their wide use in galvanic- and electroplating. These so-called superalloys offer an exceptionally high electrochemical resistance[23] if used as electrode materials, enabling a long-term use for the hydrogen evolution reaction[24,25] (HER) or for alkaline water electrolysis.[26] Resistance to corrosion[27,28] both in highly acidic or basic

* To whom correspondence should be addressed. E-mail: wendelin.stark@chem.ethz.ch. Fax: +41 44 633 10 83.

(1) Suryanarayana, C. *Int. Mater. Rev.* **1995**, *40*, 41.
(2) Makino, A.; Suzuki, K.; Inoue, A.; Masumoto, T. *Mater. Trans. JIM* **1991**, *32*, 551.
(3) Herzer, G. *Mater. Sci. Eng. A* **1991**, *133*, 1.
(4) Schiotz, J.; Di Tolla, F. D.; Jacobsen, K. W. *Nature* **1998**, *391*, 561.
(5) Haubold, T.; Bohn, R.; Birringer, R.; Gleiter, H. *Mater. Sci. Eng. A* **1992**, *153*, 679.
(6) Balaz, P.; Godocikova, E.; Kril'ova, L.; Lobotka, P.; Gock, E. *Mater. Sci. Eng. A* **2004**, *386*, 442.
(7) Ye, J.; Han, B. Q.; Lee, Z.; Ahn, B.; Nutt, S. R.; Schoenung, J. M. *Scripta Mater.* **2005**, *53*, 481.
(8) Cheung, C.; Djuanda, F.; Erb, U.; Palumbo, G. *Nanostruct. Mater.* **1995**, *5*, 513.
(9) Elsherik, A. M.; Erb, U. *J. Mater. Sci.* **1995**, *30*, 5743.
(10) Kumar, K. S.; Suresh, S.; Chisholm, M. F.; Horton, J. A.; Wang, P. *Acta Mater.* **2003**, *51*, 387.
(11) Ajdelsztajn, L.; Picas, J. A.; Kim, G. E.; Bastian, F. L.; Schoenung, J.; Provenzano, V. *Mater. Sci. Eng. A* **2002**, *338*, 33.
(12) Lu, K. *Mater. Sci. Eng. R* **1996**, *16*, 161.
(13) Gleiter, H. *Prog. Mater. Sci.* **1989**, *33*, 223.
(14) Park, J. K.; Park, K. Y.; Song, C. B. *Aerosol Sci. Technol.* **2004**, *38*, 827.
(15) Li, S. T.; Germanenko, I. N.; El-Shall, M. S. *J. Cluster Sci.* **1999**, *10*, 533.
(16) Pithawalla, Y. B.; El Shall, M. S.; Deevi, S. C. *Intermetallics* **2000**, *8*, 1225.
(17) Pithawalla, Y. B.; El-Shall, M. S.; Deevi, S. C.; Strom, V.; Rao, K. V. *J. Phys. Chem. B* **2001**, *105*, 2085.
(18) Shibata, T.; Bunker, B. A.; Zhang, Z. Y.; Meisel, D.; Vardeman, C. F.; Gezelter, J. D. *J. Am. Chem. Soc.* **2002**, *124*, 11989.
(19) Keskinen, H.; Makela, J. M.; Vippola, M.; Nurminen, M.; Liimatainen, J.; Lepisto, T.; Keskinen, J. *J. Mater. Res.* **2004**, *19*, 1544.
(20) Strobel, R.; Grunwaldt, J. D.; Camenzind, A.; Pratsinis, S. E.; Baiker, A. *Catal. Lett.* **2005**, *104*, 9.
(21) Osterwalder, N.; Capello, C.; Hungerbuhler, K.; Stark, W. J. *J. Nanopart. Res.* **2006**, *8*, 1.
(22) Mueller, R.; Madler, L.; Pratsinis, S. E. *Chem. Eng. Sci.* **2003**, *58*, 1969.
(23) Schulz, R.; Huot, J. Y.; Trudeau, M. L.; Dignardbailey, L.; Yan, Z. H.; Jin, S.; Lamarre, A.; Ghali, E.; Vanneste, A. *J. Mater. Res.* **1994**, *9*, 2998.
(24) De la Torre, S. D.; Oleszak, D.; Kakitsuji, A.; Miyamoto, K.; Miyamoto, H.; Martinez-S, R.; Almeraya-C, F.; Martinez-V, A.; Rios-J, D. *Mater. Sci. Eng. A* **2000**, *276*, 226.
(25) Kedzierzawski, P.; Oleszak, D.; Janik-Czachor, M. *Mater. Sci. Eng. A* **2001**, *300*, 105.
(26) Huot, J. Y.; Trudeau, M. L.; Schulz, R. *J. Electrochem. Soc.* **1991**, *138*, 1316.
(27) Chassaing, E.; Portail, N.; Levy, A. F.; Wang, G. *J. Appl. Electrochem.* **2004**, *34*, 1085.
(28) Xu, J.; Ai, J. H.; Xie, X. S.; Xu, Z. *Surf. Coat. Technol.* **2003**, *168*, 142.

10.1021/cm071104c CCC: $37.00
Published on Web 09/11/2007

media and an advanced wear resistance[29,30] have promoted a wide use of nickel−molybdenum alloys in coatings and resulted in components with advanced service life and excellent high-temperature performance. At present, Ni−Mo alloys are prepared in the form of micrometer-sized powders or coatings by high-energy mechanical alloying,[25,31,32] electrodeposition,[27] thermal spray,[33,34] and plasma processes.[24,35−37]

Recent measurements on the mechanical properties of nanocrystalline metal films have uncovered their exceptionally high Vickers hardness if compared to conventionally prepared materials.[13,38−42] It would be most attractive to combine the expected further increase in mechanical stability of nanocrystalline metals with the already well-established technical applications of Ni−Mo-based alloys. Grass et al. have most recently demonstrated the preparation of bulk nanocrystalline cobalt[41] by a bottom-up approach using compression and sintering of fcc-cobalt nanoparticles. The starting material was accessible in bulk quantities by reducing flame synthesis, an extension of the already industrially established classical flame aerosol processing. As previous studies on oxides[43] and salts[44,45] have showed, this production method can give access to nanoparticles with well-controlled chemical composition and particle size distribution.

The present investigation explores the preparation of complex alloys from correspondingly complex nanoparticles. The preparation of two technically most relevant Ni−Mo-based alloys, a binary superalloy (nickel, molybdenum) and a six-component Hastelloy (nickel, molybdenum, aluminum, iron, manganese, and chromium) was used to illustrate the applicability and limitations of reducing flame synthesis for the preparation of complex bulk metal−alloys. The 10−50 nm sized alloy particles were compacted to bulk nanocrystalline superalloy and compared to currently used references consisting of micrometer-sized grains. Analysis by scanning and transmission electron microscopy allowed recording of detailed electron energy loss spectra (EELS) and elemental mapping of alloy constituents and corroborated a homogeneous mixing of the metals within the alloy nanoparticles.

Experimental Section

Materials. For the preparation of metal−alloy nanoparticles the principle of the most recently developed reducing flame synthesis[44] was extended from single-component to multicomponents systems. For the synthesis of superalloy nanoparticles (Ni/Mo; see Supporting Information Table S1 for composition) an air and humidity stable liquid metal precursor was prepared from corresponding amounts of nickel 2-ethylhexanoate (6 wt % Ni) and molybdenum 2-ethylhexanoate in mineral spirits (STREM Chemicals, 15 wt % Mo). The precursor for the preparation of Nano Hastelloy (nano-Hastelloy; see Supporting Information Table S1 for composition) was prepared by additionally mixing corresponding amounts of aluminum 2-ethylhexanoate (0.8 wt % Al), manganese 2-ethylhexanoate in mineral spirits (STREM Chemicals, 6 wt % Mn), iron 2-ethylhexanoate (5.1 wt % Fe), and chromium 2-ethylhexanoate in mineral spirits (STREM Chemicals, 5.2 wt % Cr). Prior to processing the metal precursors were diluted 2:1 (w/w) with tetrahydrofurane (Fluka, tech.) and then filtered (Satorius, fluted filter type 288).

Experimental Setup. To combust the metal precursors in a controlled atmosphere under highly reducing conditions, a flame spray nozzle[46] was placed in a glovebox (see Supporting Information, Figure S1) and fed with nitrogen (PanGas, 99.999%). The atmosphere was continuously recycled by a vacuum pump (Busch, Seco SV1040CV) at about 20 $m^3\ h^{-1}$. The combustion gases H_2O and CO_2 were continuously removed from the recycle stream using two adsorption columns (zeolite 4A and 13X). An additional purge stream avoided the accumulation of other combustion-related gases (NO_x, CO, H_2). The liquid metal precursor was delivered to the spray nozzle by a micro annular gear pump (6 mL min^{-1}, HNPMikrosysteme, mzr-2900) where the liquid was dispersed by oxygen (5 l min^{-1}, PanGas tech.) and ignited by a premixed pilot flame (CH_4 1.2 L min^{-1}; O_2 2.2 L min^{-1}, PanGas tech.) surrounding the liquid spray (see Supporting Information, Figure S1). The flame was encased in a porous metal tube allowing stable combustion as suggested by Grass et al.[47,48] The product metal nanoparticles were separated from the off-gas using glass fiber filters (Schleicher&Schuell, GF6, 25.7 cm diameter), mounted on a cylinder above the exit of the reducing flame synthesis reactor. During combustion a mass spectrometer (Balzers, GAM 400) continuously monitored the concentration of the combustion gases (H_2, CO_2, H_2O, NO_x, CH_4, and O_2). The oxygen concentration in the glovebox was maintained at <100 ppm.

Powder Analysis. The as-prepared nanoparticles, Ni/Mo and nano-Hastelloy, were analyzed by X-ray diffraction (XRD; Stoe STADI-P2, G2 monochromator, Cu $K\alpha_1$, PSD detector) for crystallinity and predominant phase composition, nitrogen adsorption (BET; Tristar Micromeritics Instruments) for specific surface area and mean primary particle size, transmission electron microscopy (TEM; CM30 St-Philips, LaB_6 cathode, operated at 300 kV, point resolution ~4 Å), element microanalysis (LECO CHN-900), energy dispersive X-ray spectroscopy (EDXS), and scanning electron microscopy (SEM; FEG 1530 Zeiss Gemini). The as-prepared Ni/Mo nanoparticles were additionally analyzed by scanning transmission electron microscopy (STEM) using images obtained with a high-angle annular dark field (HAADF) detector.

(29) Wu, W. T.; Wu, L. T. *Metall. Mater. Trans. A* **1996**, *27*, 3639.
(30) Kim, H. J.; Kim, Y. J. *Surf. Eng.* **1999**, *15*, 495.
(31) Trudeau, M. L.; Schulz, R. *Mater. Sci. Eng.* **1991**, *134*, 1361.
(32) Shen, Y. P.; Hng, H. H.; Oh, J. T. *Mater. Lett.* **2004**, *58*, 2824.
(33) Dent, A. H.; Horlock, A. J.; McCartney, D. G.; Harris, S. J. *Mater. Sci. Eng. A* **2000**, *283*, 242.
(34) Sidhu, T. S.; Prakash, S.; Agrawal, R. D. *Surf. Coat. Technol.* **2006**, *201*, 273.
(35) Xu, J.; Xie, X. S.; Xu, Z.; Liu, W. J. *Mater. Chem. Phys.* **2005**, *92*, 340.
(36) Gatto, A.; Bassoli, E.; Fornari, M. *Surf. Coat. Technol.* **2004**, *187*, 265.
(37) Zhang, X.; Xie, X. S.; Yang, Z. M.; Dong, J. X.; Xu, Z.; Gao, Y.; Zhang, T. H. *Surf. Coat. Technol.* **2000**, *131*, 378.
(38) Meyers, M. A.; Mishra, A.; Benson, D. J. *Prog. Mater. Sci.* **2006**, *51*, 427.
(39) Kumar, K. S.; Van Swygenhoven, H.; Suresh, S. *Acta Mater.* **2003**, *51*, 5743.
(40) Grass, R. N.; Albrecht, T. F.; Krumeich, F.; Stark, W. J. *J. Mater. Chem.* **2007**, *17*, 1485.
(41) Grass, R. N.; Dietiker, M.; Solenthaler, C.; Spolenak, R.; Stark, W. J. *Nanotechnology* **2007**, *18*, 035703.
(42) Chokshi, A. H.; Rosen, A.; Karch, J.; Gleiter, H. *Scripta Mater.* **1989**, *23*, 1679.
(43) Madler, L.; Stark, W. J.; Pratsinis, S. E. *J. Mater. Res.* **2002**, *17*, 1356.
(44) Grass, R. N.; Stark, W. J. *Chem. Commun.* **2005**, 1767.
(45) Loher, S.; Stark, W. J.; Maciejewski, M.; Baiker, A.; Pratsinis, S. E.; Reichardt, D.; Maspero, F.; Krumeich, F.; Gunther, D. *Chem. Mater.* **2005**, *17*, 36.
(46) Madler, L.; Kammler, H. K.; Mueller, R.; Pratsinis, S. E. *J. Aerosol. Sci.* **2002**, *33*, 369.
(47) Grass, R. N.; Stark, W. J. *J. Nanopart. Res.* **2006**, *8*, 729.
(48) Grass, R. N.; Stark, W. J. *J. Mater. Chem.* **2007**, *16*, 1825.

Table 1. Particle Size and Carbon Content of Ni−Mo Alloys

samples	C[a] (wt %)	A_{BET} (m^2g^{-1})	d_{XRD}[b] (nm)	d_{BET}[c] (nm)	$\sigma_{g,n}$[d]
Ni/Mo	0.2	27.5	13	24	1.5 ± 0.03
nano-Hastelloy	0.6	32.0	13	21	1.6 ± 0.03
Reference[e]		7.6	7	87	1.5 ± 0.07

[a] Carbon content as measured by microanalysis. [b] Mean crystallite size as detected by XRD using the Scherrer formula. [c] Particle size calculated from the specific surface area,[46] error ±10% (assumed alloy density: 9 g cm^{-3}). [d] Width of the particle size distribution expressed as the geometric standard deviation of the log-normal distribution. [e] Commercial reference prepared by a metal vapor condensation method.

An energy filter (Gatan imaging filter, GIF) installed below the Technai 30 FEG allowed recording electron energy loss spectra (EELS) of all samples and element-specific images (elemental maps) of Ni/Mo by means of the electron spectroscopic imaging (ESI) technique. The thermal stability and metal content was quantitavely followed by a thermobalance (Linseis TG/STA-PT1600, 25−750 °C, 10 °C/min) under air or H_2 in argon (7 vol % H_2, PanGas). The thermobalance was coupled to a mass spectrometer (Thermostar, Balzers) for analysis of the evolving gases. For comparison, Hastelloy C276 (Aldrich, nanopowder) was used as the closest commercially available reference material (reference; see Supporting Information Table S1 for composition).

Vickers Hardness. Both nanocrystalline samples and reference material were investigated for their mechanical properties by pressing the as-prepared metal powders into pills with a diameter of 1.2 cm, using a uni-axial press at 370 MPa for 5 min. The pills were sintered under H_2 in argon (7 vol % H_2, PanGas) at 900 °C for 30 min and their Vickers hardness was measured using a Brickers 220 (Gnehm, Horgen) at a test load of 0.3 kg after embedding the pills in Bakelite at 180 °C and 20 kN for 6 min.[47]

Results

Ni−Mo-Based Alloy Preparation. The spray flame combustion of the metal 2-ethylhexanoate precursors[48−50] under a nitrogen atmosphere resulted in the production of lightweight black powders at 18 g h^{-1}. Mass spectroscopy analysis during all runs confirmed that the oxygen levels remained below 100 ppm during the production of the nanoparticles. Element microanalysis confirmed that the formation of undesired soot could be avoided in both alloys (Ni/Mo; 0.2 wt % carbon, nano-Hastelloy; 0.6 wt % carbon; Table 1). This carbon level was insufficient to attribute it to the formation of carbon layers surrounding the nanoparticles. Transmission electron microscopy (TEM) confirmed that the material consisted of nearly spherical nanoparticles of 10−50 nm (Figure 1a,b). The best available commercial reference material (Reference) consisted of much bigger particles of about 100 nm size with some particles larger than 200 nm (Figure 1c). While Ni/Mo superalloy could be produced as a homogeneous material (Figure 1a), Figure 1b showed that the nano-Hastelloy nanoparticles consisted of two different components (Figure 1b, arrow).

Element Distribution. Energy-dispersive X-ray spectroscopy (EDXS) followed by scanning transmission electron microscopy (STEM) identified that Ni/Mo contained only metal nickel and molybdenum nanoparticles (see Supporting Information, Figure S2) whereas nano-Hastelloy consisted of nickel/molybdenum alloy and alumina nanoparticles, as a nonuniform material (see Supporting Information, Figure S3). The other low content metals (Fe, Mn, and Cr) could be not detected, reflecting the relative low detection limits of EDXS. On the other hand, the EDXS and STEM analysis of the reference material (see Supporting Information, Figure S4) confirmed the presence of a majority of the metallic components in spite of their low concentration (see Supporting Information, Table ST1).

Particle Size Distribution. The metal nanoparticles made by reducing flame synthesis exhibited a much higher surface area (Table 1, Ni/Mo 27.5 m^2 g^{-1}; nano-Hastelloy 32.0 m^2 g^{-1}) than the commercial reference material (reference 7.6 m^2 g^{-1}). The volume-based particle size distribution of the samples was evaluated by visual particle counting of at least 500 particles (Figure 2) assuming that all particles were spherical. The results could be fitted to a log-normal distribution with a number-based geometric standard deviation for every sample (Table 1). Indicated by the TEM observation, the volume-based distribution of the reference material was very wide. In contrast, the alloy nanoparticles prepared by reducing flame synthesis had a relatively narrow particle size distribution with an average particle size of about 35 nm. The particle size distribution as derived from TEM observations can be confirmed by specific surface area measurements (Table 1) using nitrogen adsorption at −196 °C following the BET method yielding the corresponding calculated particle size diameter d_{BET} (Table 1).

Crystal-Phase Composition. The identity of the alloy phase of Ni/Mo was investigated by element mapping on a transmission electron microscope (Figure 3a). Although the sensitivity of the nickel mapping is much higher than for molybdenum, nickel (Figure 3b) and molybdenum (Figure 3c) always occurred together and corroborated the successful preparation of non-noble-metal−alloy nanoparticles. The X-ray diffraction (XRD) pattern of the as-prepared nanomaterial was compared to the one of the reference material and corroborated the formation of the metal nickel−molybdenum alloy nanoparticles (Figure 4). No sign of the formation of oxides or carbide species could be observed. Heating the nanoalloy under air resulted in oxidation of the samples and the formation of the thermodynamically favored NiO and $Ni(MoO_4)$. In contrast to the specific surface area derived particle size, the mean crystallite diameter of the reference material as determined from the peak width using the Scherrer formula was significantly smaller than the mean particle diameter (Table 1), indicating polycrystalline particles as further discussed below.

Thermal Stability and Metal Content. The thermal stability of the flame-made metal−nanoalloys was determined through thermogravimetric analysis. Both samples remained fully stable up to approximately 190 °C under air and ignited spontaneously at about 245 °C, resulting in a mass gain of about 18.5 wt % (Figure 5a). This was followed by a slow oxidation resulting in a total mass gain of 27.8 wt % for Ni/Mo and 26.8 wt % for nano-Hastelloy. From the thermogravimetric data the metal content of the as-prepared

(49) Stark, W. J.; Madler, L.; Maciejewski, M.; Pratsinis, S. E.; Baiker, A. *Chem. Commun.* **2003**, 588.
(50) Athanassiou, E. K.; Grass, R. N.; Stark, W. J. *Nanotechnology* **2006**, *17*, 1668.

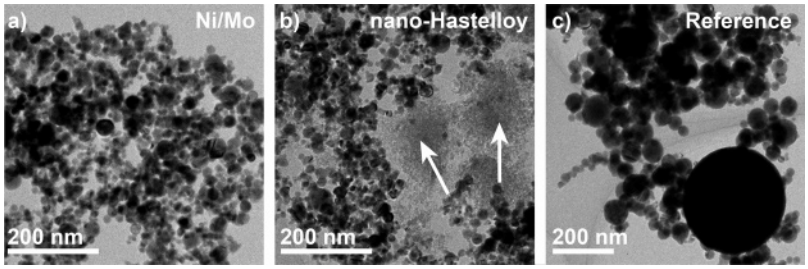

Figure 1. Transmission electron micrographs (TEM) of the as-prepared materials. Reducing flame synthesis resulted in almost spherical 10−50 nm sized particles of the metal−alloys (a, b) Ni/Mo and nano-Hastelloy. In the case of nano-Hastelloy heterogeneous nucleation of distinct nickel−molybdenum and alumina-based oxide particles occurred, as confirmed by electron energy loss spectra (see Supporting Information, Figure S3). Currently used metal Hastelloy powders contain large particles as dominant constituents and cannot be defined as nanoparticles (c).

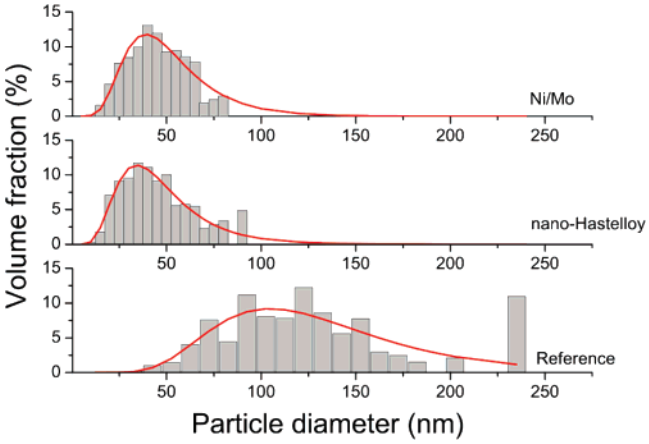

Figure 2. Particle size distributions evaluated from electron micrographs of as-prepared materials (500 particles) and fits to a log-normal distribution. The commercial reference (made by metal vapor condensation) consists of much bigger particles than the nanoparticles accessible through reducing flame synthesis.

Ni/Mo nanoparticles could be computed to 82.2 wt % and the oxygen content 4.6 wt % assuming full oxidation of nickel to NiO and molybdenum to MoO_3 (theoretical mass gain 33.8 wt %). As a low carbon content was present (Table 1), it could be assumed that the diminished mass gain could be attributed to the presence of oxide layers covering the nanoparticles. Since only few carbon was present in the samples (Ni/Mo: 0.2 wt % C; Table 1), the mass loss during the thermogravimetric measurements (Figure 5) can be attributed to oxygen leaving the sample in the form of water. This was confirmed by mass spectroscopy (see Supporting Information, Figure S5, second trace). From the mass gain during oxidation, the oxygen content of the samples could be calculated to 4.6 wt %. During preparation of three-dimensional samples, sintering of the Ni/Mo alloy nanoparticles under H_2 in argon (7 vol % H_2) resulted first in the reduction of the oxide species at around 300 °C (Figure 5; total mass loss of 4.7 wt %) before sintering and particles growth of the alloy particles consolidated the sample. The oxygen content of 4.7 wt % stays in agreement with the calculated content (4.6 wt %) and with the hydrogen consumption during reduction (0.17 ± 0.03 mmol of H_2; see Supporting Information, Figure S5). The surface of the Ni/Mo nanoparticles was further investigated by TEM and revealed the presence of an amorphous layer covering the metal nanoparticles (Figure 5b, arrows). This layer can therefore be attributed to 5−7 nm oxides covering the metallic alloy core.

Mechanical Properties and Bulk Nanocrystalline Alloy Preparation. Pressing the free-flowing powders uniaxially at 370 MPa and subsequent sintering resulted in centimeter-sized metallic disks with a characteristic metallic gloss and reflectivity. Table 2 shows that Ni/Mo and nano-Hastelloy displayed a strongly enhanced Vickers hardness if compared to Reference, bulk Hastelloy B-2 and other Ni-based alloys. Earlier studies report that a combination of mechanical alloying and spark plasma sintering of a nickel/molybdenum-rich alloy resulted in a nanocrystalline material[24] with similar microhardness properties but high inhomogeneity. Thin film coatings of nickel molybdenum alloys produced by electrodeposition also afforded nanomaterials[27] with high microhardness depending on their molybdenum content. The present work extends the range of material geometries by allowing three-dimensionally extended objects while thin film deposition is an excellent method for the preparation of coatings.

Micromorphology and Homogeneity. To better study the origin of these properties, the morphology of the nanocrystalline pills was examined by scanning electron microscopy (SEM). Upon compaction of the as-prepared powders the particles rearranged, giving a density close to the limit of freely flowing spheres (relative density: ≈60%) without any change in the particle size or shape (see Supporting Information, Figure S6). No macroscopic difference (optical appearance) was observed between the three samples. Sintering under H_2 in argon (7 vol % H_2) at 900 °C yielded nanocrystalline materials with an enhanced Vickers hardness (Ni/Mo: 760 HV, nano-Hastelloy: 800 HV) and a denser but different surface morphology (Figures 6a and 7). Scanning electron microscopy revealed that the surface of the Ni/Mo pill became rougher as sintering favored the formation of sintering necks and bigger grains (∼150−300 nm) with a particular crystal structure (Figure 7). A detailed surface analysis of the Ni/Mo revealed the presence of predominantly polycrystalline particles with a unique parallel structure and the formation of twins (Figure 7 arrow).

In contrast to the binary Ni/Mo, the chemically more complex nano-Hastelloy did not display formation of such large particles or grains (Figure 6a) and showed a smooth and homogeneous surface structure. The reference (conventional Hastelloy) pills had an irregular structure (Figure 6b) of a highly grainy appearance and no single particles were discernible. This highly heterogeneous structure reflects the poor particle size distribution of the starting material (Figure 2).

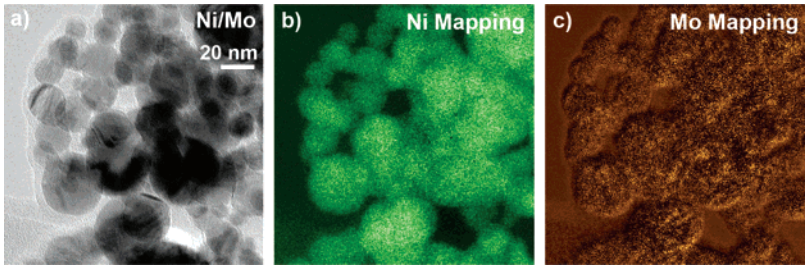

Figure 3. Element distribution and homogeneity of as-prepared Ni/Mo alloy. (a) Transmission electron micrographs (TEM) of the as-prepared material revealed spherical particles with a 5 nm oxide coating (see Figure 5). The distribution of the elements is shown by mapping the nickel (b) and the molybdenum (c) concentration using an energy-dispersive X-ray detector. Additional analysis of single nanoparticles are available in the Supporting Information (Figures S2−S4).

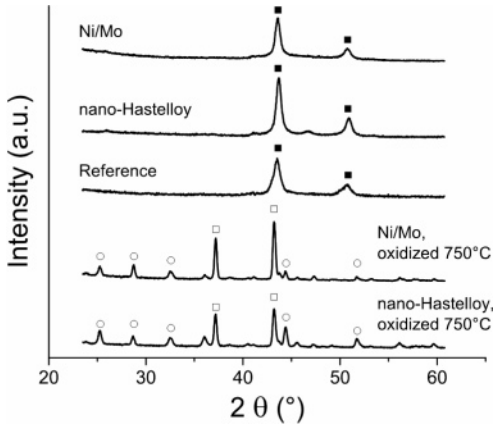

Figure 4. X-ray diffraction pattern of the as-prepared material confirmed the presence of the metal nickel−molybdenum alloy (■). No additional peaks of other metallic or oxidic species could be detected for nano-Hastelloy. Heating the as-prepared materials under air to 750 °C resulted in the oxidation of the alloy and formation of NiO (□) and Ni(MoO_4) (○).

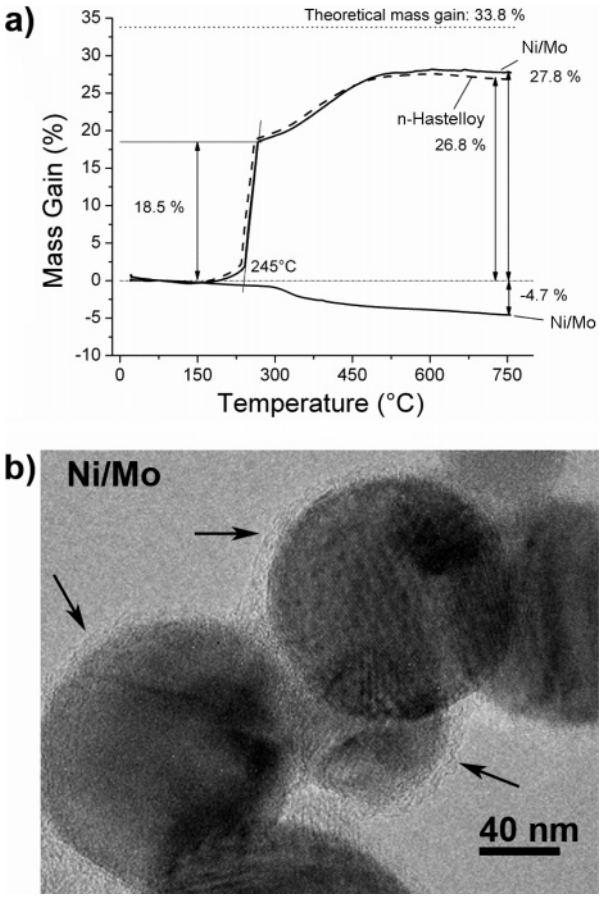

Figure 5. Thermogravimetric analysis of Ni/Mo and nano-Hastelloy. Oxidation of the nanopowders under air resulted in a mass gain of approximately 27 wt % (a). Sintering of Ni/Mo under H_2 in argon (7 vol % H_2) revealed that the nanoparticles were covered by a thin oxide layer that could be reduced to water. This core−shell structure was corroborated by TEM images (b). The thickness of the oxide layer is about 5−7 nm (b, arrows) and stays in agreement with the oxide content (see Supporting Information, Figure S5).

Discussion

Nanocrystalline Alloy Preparation. *Metal−Alloy Nanoparticles.* Conventional flame aerosol synthesis today accounts for the industrial manufacturing of several million tons of oxides and carbon black, annually. The present work shows how suitable modifications of flame synthesis allow preparation of a much broader range of products including complex non-noble-metal−alloys. The use of oxygen-limited flames allows controlled aerosol production in highly reducing environments. In principle, the classical ore reduction processes can also run in the form of aerosols in a flame where the chemistry and thermodynamics stay similar. We have demonstrated this by using two examples: Single-phase metal nickel−molybdenum nanoparticles (superalloy: Figures 1a and 3a) and a six-component nano-Hastelloy (Figure 1b) made accessible at production rates of about 18 g h^{-1} on laboratory-scale reactors. The Hastelloy composition offers an excellent example for studying the range of accessible products since it contains metals ranging from relatively noble (Ni) to highly electronegative like aluminum. This provides the basis for a detailed thermodynamic analysis as given in the section below.

Mechanism. The reducing flame process presented here affords nanoparticles with a mean primary particle diameter of about 35 nm and a relative narrow particle size distribution (Figure 2). The similarity of this preparation method to the industrially used flame aerosol process can well be recognized from the log-normal shape of the particle size distribution. The number-based geometric standard deviation (Table 1) is in close agreement with modeling results based on Brownian aggregation of nanoparticles in the gas phase as investigated in detail for oxide nanoparticle[51,52] manufacturing. In contrast to this, the presence of 200−300 nm particles (Figure 1c) in currently available commercial Hastelloy powders illustrate the result of an ill-controlled manufacturing process.

(51) Vemury, S.; Pratsinis, S. E. *J. Aerosol. Sci.* **1995**, *26*, 175.
(52) Dekkers, P. J.; Friedlander, S. K. *J. Colloid Interface Sci.* **2002**, *248*, 295.

Table 2. Microhardness of Ni−Mo-Rich Alloys Prepared by Different Processes

samples	phase composition	production method	hardness[a] (HV)	load (kg)	reference
Ni/Mo	$Ni_{70}Mo_{30}$	reducing flame synthesis	760	0.3	this work
nano-Hastelloy	$Ni_{79}Mo_{14}$/ceramic phase	reducing flame synthesis	800	0.3	this work
Reference		evaporation/condensation	680	0.3	this work
Ni−Mo alloy	$Ni_{80}Mo_{20}$	plasma nitriding	330	0.01	76
Ni−Mo alloy	$Ni_{70}Mo_{30}$	electrodeposition	650	0.05−0.2	27
Ni−Mo alloy	γ-Ni/CrB/Cr_7C_3	laser cladding	730	1	55
Ni−Mo alloy	γ-Ni/CrB/Cr_7C_3	plasma cladding	500	1	55
Ni−Mo-rich alloy	Ni/Mo/MoO_2 and other phases	mech. alloying; spark plasma sintering	785−950	10	24
bulk Hastelloy B-2	$Ni_{67}Mo_{28}Co_1Cr_1Mn_1$		290		27
bulk Hastelloy C-276	metallic phase	plasma transferred arc	220		36

[a] The unit of hardness is known as the Vickers Pyramid Number (HV): 1 HV = 9.807 MPa.

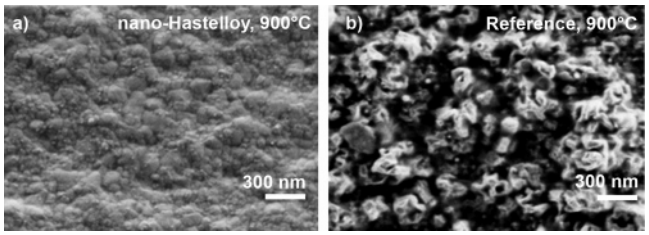

Figure 6. Scanning electron microscopy (SEM) images of uniaxially pressed pills of nano-Hastelloy (a) and a reference material (b) with ill-defined particle size distribution (Figure 2). Sintering of the pills under H_2 in argon (7 vol % H_2) to 900 °C resulted in a homogeneous smooth surface containing bigger grains and sintering necks (a). Sintering of the commercial reference powder resulted in a more porous and rough surface (b).

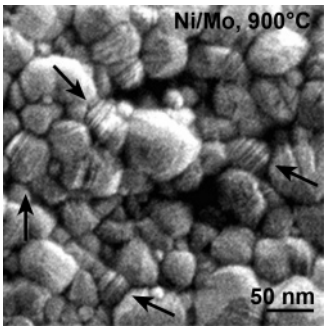

Figure 7. Scanning electron microscopy (SEM) image of a pill of Ni/Mo sintered at 900 °C under H_2 in argon (7 vol % H_2). Sintering resulted in the formation of crystal twins which contribute to the enhanced microhardness.

Air Stability. Both Ni/Mo and Hastelloy nanoparticles exhibited an unexpected high air stability, which stays in contrast to the pyrophoric nature of most ultrafine metal nanopowders. Such passivation has been already traced to the presence of carbon shells on metal nanoparticles[50,53] but could be excluded in the present materials based on microanalysis measurements (C content: <0.6 wt %). Thermogravimetric analysis (see Supporting Information, Figure S5) and transmission electron micrographs corroborated the presence of an amorphous 5−7 nm nickel/molybdenum oxide layer, protecting the nanopowder from ignition at room temperature and total oxidation. This lies in agreement with other studies on the production of Hastelloy[54] or FeAl alloy nanoparticles[17] protected by an amorphous oxide coating. We assume that this core/shell structure was formed by partial oxidation of the metallic core within the cooler parts of the flame (see theoretical considerations below). Comparing the mass gain or loss of Ni/Mo (Figure 5a) and nano-Hastelloy during oxidative or reductive heating in a thermobalance to the calculated total mass gain expected from complete oxidation of the metallic material stays in agreement with the chemical composition of the material (see Supporting Information, Table S1) and the presence of previously oxidized constituents such as alumina and chromia (Figure 1b). The detailed analysis confirmed that reducing flame synthesis could give access to uniform nanoparticles (see Supporting Information, Figure S2−S4 for element distributions in single nanoparticles) consisting of a single, well-defined metallic core (Figure 4) excluding mixed metallic[24] or carbide phases[35] as previously seen during plasma or laser cladding[55] or mechanical alloying followed by spark plasma sintering.[24] The primary particle diameters from all investigated materials stayed in full agreement with electron micrographs. This analysis revealed the broad and poorly defined structure of currently produced sub-micrometer Hastelloy (Reference) displaying large particles (Figure 1) and a corresponding broad particle size distribution (Figure 2). A comparison of mean crystallite sizes d_{XRD} (Table 1) to primary particle sizes revealed the presence of polycrystalline particles and stays fully in line with the observed formation of twins (Figure 7).

Bulk Nanocrystalline Alloys. The presence of a thin passivating layer on the alloy nanoparticles did not interfere with their use as a starting material for the preparation of bulk nanocrystalline alloys. Sintering of the as-prepared powders under H_2 in argon (7 vol % H_2) resulted in nanocrystalline materials with exceptional microhardness properties. Previous work on grain growth in nickel-based alloys prepared by mechanical alloying[56] and by electrodeposition[57] showed significant grain growth with average sizes of about 150 nm for temperatures above 500−600 °C. The mass spectroscopy data of the sintering step under 7 vol % H_2 in argon confirmed that the oxide shell reduced at much lower temperature (see Supporting Information, $T \approx 275-400$ °C; Figure S5) than the sintering of the material and therefore allows an in situ removal of the oxide layer and

(53) Grass, R. N.; Athanassiou, E. K.; Stark, W. J. *Angew. Chem., Int. Ed.* **2007**, *46*, 4909.
(54) Zocco, A.; Perrone, A.; Vignolo, M. F.; Duhalde, S.; Avram, I.; Morales, C.; Perez, T. *Appl. Surf. Sci.* **2003**, *208*, 669.
(55) Xu, G. J.; Kutsuna, M.; Liu, Z. J.; Zhang, H. *Mater. Sci. Eng. A* **2006**, *417*, 63.
(56) Datta, M. K.; Pabi, S. K.; Murty, B. S. *Philos. Mag. Lett.* **2001**, *81*, 77.
(57) Chang, L.; Kao, P. W.; Chen, C. H. *Scripta Mater.* **2007**, *56*, 713.

subsequent sintering in the same process step. The strong increase in hardness upon sintering may be predominantly attributed to an increase in density and limited crystallite growth,[13,58] as most recently investigated in detail for nanocrystalline nickel[10] and cobalt[41] prepared from fcc-cobalt nanoparticles. In the case of Ni/Mo a high density of twinning effects was visible (Figure 7). Both theoretical predictions and experimental investigations[38,39,59,60] have suggested that such twinning effects and twin boundaries may result in a significant strengthening of nanocrystalline bulk metals and alloys. Our findings confirm this for nanocrystalline bulk samples of Ni/Mo alloys. Similar to Ni/Mo superalloy, the advanced hardness properties of nano-Hastelloy can be attributed to the limited grain growth after sintering up to 900 °C (Figure 6a). The presence of the alumina ceramic phase[61] may contribute in addition to limiting the crystallite growth of the nanoparticles, resulting in an even slightly increased Vickers hardness if compared to Ni/Mo (Table 2). This observation agrees with recent studies where a second oxide phase has been used for dispersion hardening[62,63] and with the most recent observation of an up to 5-fold increase in Vickers hardness for nanocrystalline bismuth metal upon intimate mixing with ceria nanoparticles.[40] More generally speaking, most alloys contain significant amounts of ceramics to combine beneficial properties from both constituents.[64,65] Nanocrystalline metals strongly profit from the presence of a ceramic phase since the latter hinders the grain growth of the nanocrystalline metal phase and results in advanced thermal properties (less sintering). The ill-structured surface of the reference (Figure 6b) material correlates with the inferior Vickers hardness, the broad particle size distribution of the starting material, and the presence of large particle impurities.

Materials exhibiting high hardness and relative high ductility are most attractive for structural and engineering applications. For most nanocrystalline (grain size <100 nm) and ultrafine polycrystalline (grain size between 100 nm and 1 μm) materials, it has been extensively shown that smaller grain size provokes a higher yield strength and lowers the uniform elongation. Since the uniform elongation is generally low, this results in materials with a high hardness (Hall-Petch relationship) but lower toughness and lower ductility.[38,66]

Recent studies of nanocrystalline materials (grain size <100 nm) prepared by cryo-milling[67,68] have resulted in materials with both a high hardness and high toughness. The consolidation step was described as the crucial step for achieving these attractive material properties. Obviously, the consolidation parameters have to result in a porous and defect-free structure in which the particles are ideally bonded with each other. Even minor flaws in the structure could strongly downgrade the ductility properties of the material. A low ductility is expected for the present material due to the presence of twinning effects (Ni/Mo, Figure 7) and even supported by the presence of a second ceramic phase (nano-Hastelloy, Figure 1b). Further investigations, particularly on the consolidation step, are required to further improve the present nanocrystalline materials. An alternative strategy was proposed by Wang et al.[69] reporting on the preparation of a material with bimodal or multimodal grain size distribution. The preparation of a composite of nanocrystalline particles with small ($\approx$100 nm) and much bigger grains (classical alloy powders; size ≈ 1 μm) would be expected to result in strain hardening. Such combinations of classical and nanopowders are therefore amenable for the fabrication of parts with higher toughness.

Process Limitations. The successful earlier flame aerosol preparations of cobalt, bismuth, and copper and the extension presented here to complex metal−alloys are motivation for a more in-depth analysis of the accessible range of products by this rapid gas-phase process. Any constituents entering a flame reactor will experience a specific temperature history with different chemical constituents present in the surrounding gas phase. Similar temperatures and compositions are found at a much larger scale in conventional ore processing. Therefore, the individual chemical species and the involved thermodynamics can be adapted from classical high temperature ore chemistry and metallurgy. Since the here reported flame process is oxygen-limited, all metals and the gaseous species H_2 and CO compete for the remaining oxygen or stay in a continuous redox equilibrium while passing the hot phase of the reactor.

Ellingham Diagrams. To analyze these complex interactions, we computed an Ellingham diagram based on the corresponding $\Delta_r G$ values of the different constituents (see Supporting Information, Figure S7). Aluminum, chromium, and manganese are more readily oxidized than CO, H_2, iron, nickel, and molybdenum. This ranking was consistent for the whole temperature range from 25 to 1500 °C and reflects the less negative reaction enthalpy ($\Delta_r H°$) of the oxidations of nickel and molybdenum if compared to the values of aluminum, manganese, or chromium. While care should be taken to consider flames to operate at fully established thermodynamic equilibrium,[70] the calculated possible formation of metallic nickel or molybdenum stays in full agreement with our experimental findings. The impossibility to reduce alumina, chromia, or manganese oxide further confirms the validity of this analysis (see Supporting Information, Figure S3).

(58) Hall, E. O. *Nature* **1954**, *173*, 948.
(59) Lu, L.; Sui, M. L.; Lu, K. *Science* **2000**, *287*, 1463.
(60) Manusmare, P. G.; Leighly, H. P. *Acta Metall.* **1976**, *24*, 1047.
(61) Zhang, Z. F.; Zhang, L. C.; Mai, Y. W. *Wear* **1994**, *176*, 231.
(62) Naser, J.; Riehemann, W.; Ferkel, H. *Mater. Sci. Eng.* **1997**, *234*, 467.
(63) Redsten, A. M.; Klier, E. M.; Brown, A. M.; Dunand, D. C. *Mater. Sci. Eng. A* **1995**, *201*, 88.
(64) Sarkar, P.; Datta, S.; Nicholson, P. S. *Composites Part B* **1997**, *28*, 49.
(65) Dieringa, H.; Huang, Y. D.; Maier, P.; Hort, N.; Kainer, K. U. *Mater. Sci. Eng. A* **2005**, *410*, 85.
(66) Li, S. X.; Cui, G. R. *J. Appl. Phys.* **2007**, *101*, 083525.
(67) Cheng, S.; Ma, E.; Wang, Y. M.; Kecskes, L. J.; Youssef, K. M.; Koch, C. C.; Trociewitz, U. P.; Han, K. *Acta Mater.* **2005**, *53*, 1521.
(68) Youssef, K. M.; Scattergood, R. O.; Murty, K. L.; Horton, J. A.; Koch, C. C. *Appl. Phys. Lett.* **2005**, *87*, 091904.
(69) Wang, Y. M.; Ma, E. *Acta Mater.* **2004**, *52*, 1699.
(70) Brink, A.; Kilpinen, P.; Hupa, M.; Kjaldman, L. *Combust. Sci. Technol.* **1999**, *141*, 59.

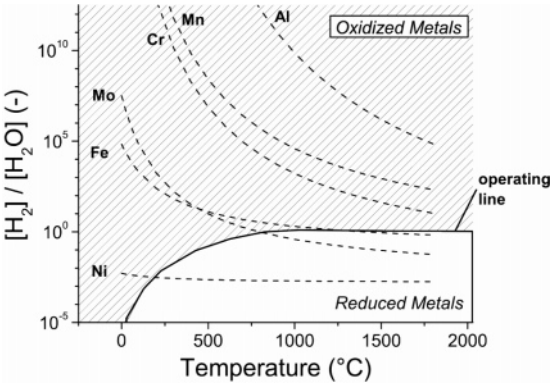

Figure 8. Thermodynamic calculations in the form of an Ellingham diagram (see Supporting Information, Figure S7) allow discussion of accessible alloys and metals. The lines which lay below the flame process operating line indicate accessible metals at the corresponding temperature (nickel, molybdenum, and iron above 1500 °C). Others, such as alumina, are not accessible in a CO/H_2 system.

Accessible Metals and Alloys. To further analyze possible future extensions of flame aerosol synthesis, we calculated the $[H_2]/[H_2O]$ ratios that would allow reduction of specific metals and included the operation line of the here used reactor in the plot (Figure 8) using experimentally confirmed hydrogen and water concentrations (flame off-gas analysis by mass spectroscopy).[48] Figure 8 shows that all lines which cross and lay below the operating line corresponded to metal species that can be produced in their reduced (metal) form. Again, this result stays in agreement with the experimental findings. The observed heterogeneous nucleation of alumina and Ni/Mo (Figure 1b) can be attributed to a lack of wetting of metals on alumina and vice versa. This mechanistic observation also agrees with earlier investigations on the simultaneous preparation of noble metal and oxide nanoparticles by classical flame spray synthesis.[71−75]

Conclusion

The present study illustrates how oxygen limitation allowed an extension of classical flame aerosol processing to access metal and alloy nanoparticles. From a product engineering point of view, further investigations on both process and product will be required before the here-described process can be extended to the industrial-scale manufacturing of nanocrystalline metals. However, the present work has shown that bulk nanocrystalline alloys can readily be prepared by a bottom-up approach using corresponding metal nanoparticles and that such materials display the predicted advanced mechanical properties. With its capability to access three-dimensional objects of complex shape, this bottom-up approach may offer a possible alternative to electrodeposition or plasma processes for the fabrication of specific three-dimensional objects of nanocrystalline alloys.

Acknowledgment. The authors thank Dr. F. Krumeich and the Electron Microscopy Center of ETH Zurich (EMEZ) for the transmission microscopy imaging and energy-dispersive X-ray spectroscopy. Financial support by the ETH Zurich and SNF grant 200021-116123/1 are gratefully acknowledged.

Supporting Information Available: Experimental setup for the preparation of non-noble-metal−nanoalloys (Figure S1) by reducing flame synthesis; energy-dispersive X-ray spectroscopy of Ni/Mo (Figure S2), nano-Hastelloy (Figure S3), and reference material (Figure S4); thermal stability and oxygen content of Ni/Mo (Figure S5); scanning electron microscopy images of a uniaxially pressed pill made of as-prepared Ni/Mo (Figure S6); Ellingham diagram and thermodynamic calculations (Figure S7). This material is available free of charge via the Internet at http://pubs.acs.org.

CM071104C

(71) Keskinen, H.; Makela, J. M.; Aromaa, M.; Keskinen, J.; Areva, S.; Teixeira, C. V.; Rosenholm, J. B.; Pore, V.; Ritala, M.; Leskela, M.; Raulio, M.; Salkinoja-Salonen, M. S.; Levanen, E.; Mantyla, T. *Catal. Lett.* **2006**, *111*, 127.
(72) Stark, W. J.; Grunwaldt, J. D.; Maciejewski, M.; Pratsinis, S. E.; Baiker, A. *Chem. Mater.* **2005**, *17*, 3352.
(73) Makela, J. M.; Keskinen, H.; Forsblom, T.; Keskinen, J. *J. Mater. Sci.* **2004**, *39*, 2783.
(74) Strobel, R.; Krumeich, F.; Stark, W. J.; Pratsinis, S. E.; Baiker, A. *J. Catal.* **2004**, *222*, 307.
(75) Strobel, R.; Stark, W. J.; Madler, L.; Pratsinis, S. E.; Baiker, A. *J. Catal.* **2003**, *213*, 296.
(76) Makishi, T.; Nakata, K. *Metall. Mater. Trans. A* **2004**, *35A*, 227.